Evaluating the role of solar photovoltaic and battery storage in supporting electric aviation and vehicle infrastructure at Visby Airport

Applied Energy 352 (2023) 121946

Contents lists available at ScienceDirect

Applied Energy

journal homepage: www.elsevier.com/locate/apenergy

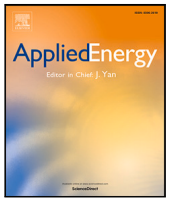

Evaluating the role of solar photovoltaic and battery storage in supporting electric aviation and vehicle infrastructure at Visby Airport

Patrik Ollas [a,b,*], Sara Ghaem Sigarchian [a], Hampus Alfredsson [c], Jennifer Leijon [d], Jessica Santos Döhler [d], Christoffer Aalhuizen [d], Torbjörn Thiringer [b], Karin Thomas [d]

[a] Department of Energy and resources, RISE Research Institutes of Sweden, Borås, Sweden
[b] Department of Electrical Engineering, Chalmers University of Technology, Göteborg, Sweden
[c] Department of Mobility and Systems, RISE Research Institutes of Sweden, Göteborg, Sweden
[d] Department of Electrical Engineering, Uppsala University, Uppsala, Sweden

ARTICLE INFO

Keywords:
Airport
Electric aviation
Battery storage system
Solar photovoltaic
Battery control
Techno-economic analysis

ABSTRACT

Following the societal electrification trend, airports face an inevitable transition of increased electric demand, driven by electric vehicles (EVs) and the potential rise of electric aviation (EA). For aviation, short-haul flights are first in line for fuel exchange to electrified transportation. This work studies the airport of Visby, Sweden and the effect on the electrical power system from EA and EV charging. It uses the measured airport load demand from one year's operation and simulated EA and EV charging profiles. Solar photovoltaic (PV) and electrical battery energy storage systems (BESS) are modelled to analyse the potential techno-economical gains. The BESS charge and discharge control are modelled in four ways, including a novel multi-objective (MO) dispatch to combine self-consumption (SC) enhancement and peak power shaving. Each model scenario is compared for peak power shaving ability, SC rate and pay-back-period (PBP). The BESS controls are also evaluated for annual degradation and associated cost. The results show that the novel MO dispatch performs well for peak shaving and SC, effectively reducing the BESS's idle periods. The MO dispatch also results in the battery controls' lowest PBP (6.9 years) using the nominal economic parameters. Furthermore, a sensitivity analysis for the PBP shows that the peak power tariff significantly influences the PBP for BESS investment.

1. Introduction

1.1. Background

In the EU, the total emissions from aviation in 2017 accounted for 3.8% of the total CO_2 emissions, with 13.9% of the emissions from transport, making it the second largest emitter of transport greenhouse gas (GHG) after road transport [1]. If global aviation were a country, it would rank among the top ten emitters. Before the Covid pandemic, the International Civil Aviation Organization forecasted that the emissions could triple by 2045 compared to 2015 [2]. Aviation is vital for urban development [3], and electric-driven aircraft is a potential solution measure to reduce aviation-derived emissions. Electric aviation (EA) would significantly reduce the environmental impact and eliminate CO_2 and non-CO_2 emissions while reducing noise. With today's technology, short-haul flights (less than 1500 km) are best suited for electrified aircraft with zero in-operation emissions. In 2019, these fossil-driven short-haul flights accounted for one-third of the passenger CO_2 emissions [4].

Budd et al. examined how UK airports address the challenge of reducing the environmental impacts of operations and listed the identified sustainable practices [5]. The study also highlights the current demographic differences in implementation pace and stresses the importance of emerging markets following the leading examples. Airport authorities and managers are increasingly paying attention to the sustainability implications of airport design [6].

Airports require vast and flat areas for their operation, with large open fields along the runway to offer safe take-offs and landings, and usually with a sound buffer area to reduce noise pollution. The energy consumption of a larger airport is equivalent to a six-digit population city with around-the-clock energy demand, putting significant stress on the electricity grid. A potential grid stress relief is deploying solar photovoltaic (PV) arrays on open, flat, and—in many cases—shading-free spaces. Santa et al. analyse which sustainability practices are used at airports today through a literature review, aiming to propose a sustainable airport model [7]. Ten indicators were identified, including

* Corresponding author at: Department of Energy and resources, RISE Research Institutes of Sweden, Borås, Sweden.
E-mail address: patrik.ollas@ri.se (P. Ollas).

https://doi.org/10.1016/j.apenergy.2023.121946
Received 12 May 2023; Received in revised form 4 September 2023; Accepted 10 September 2023
Available online 19 September 2023

Nomenclature

δ_{soc}	Adjustable term for minimum SOC
κ	Conditional term for battery MO operation
$\mathbb{C}_{batt}$	Relative battery price ($/kWh)
$\mathbb{C}_{bought}$	Electricity buy price
$\mathbb{C}_{cert}$	Electricity certificate price
$\mathbb{C}_{deg}$	Monetised battery degradation
$\mathbb{C}_{net}$	Net electricity bill
$\mathbb{C}_{NS}$	Nordic electricity hourly spot price
$\mathbb{C}_{peak}$	Annual cash savings from peak shaving
$\mathbb{C}_{pv}$	Relative PV price ($/kW)
$\mathbb{C}_{sold}$	Electricity selling price
$\mathbb{C}_{tax}$	Electricity surcharge
$\mathbb{C}_{tax}$	Electricity tax price
$\mathbb{C}_{t}$	Peak power tariff
$\mathbb{C}_{var}$	Variable grid charge
I_0^x	Initial system investment, x PV $\vee$ battery
i_{batt}	Battery current
i_{cell}	Battery cell current
$n(t)$	Battery cycle number
p_{batt}	Battery power
p_{ch}^{EA}	SOC-dependent charging power
p_{net}	Net grid power
p_{sh}	Peak shaving power
p_{Sx}^{m}	Monthly peak power for S_x
pv_{exp}	PV export (to the grid)
q_{batt}	Battery charge level
q_{loss}	Battery cycle ageing degradation
soc_{min}^{sv}	Seasonal variation of minimum SOC
u_{batt}	Battery voltage
u_{OCV}	Open-Circuit Voltage
A_h	Battery capacity throughput
ALR	Array-to-Load
B	Pre-exponential degradation factor
BAU	Business As Usual
BESS	Battery Energy Storage System
CF_{ac}	EA cabin factor
DoD	Depth of discharge
E_a	Activation energy
E_{batt}	Battery size (energy)
E_{pv}	PV annual energy yield
EA	Electric Aviation
EFC	Equivalent full cycles
EV	Electric Vehicle
m_{string}	No. of parallel strings
MILP	Mixed Integer Linear Programming
MO	Multi-objective
n_{cell}	No. of series-connected cells
N_{EA}	EV arrivals before EA departure
N_{pax}^{veh}	Passengers per EV
N_{seat}^{ac}	EA seating capacity
OCV	Open-Circuit Voltage
P_{batt}	Maximum battery power
P_{load}^{avg}	Annual average load demand
P_{PV}	PV array rated power
PBP	Pay-back-period
PV	Solar photovoltaic
PV_n	PV array for location $n \in 1{:}3$
Q_{batt}^{rated}	Battery rated capacity
Q_{cell}	Cell nominal capacity
R	Ohmic Resistance
R_g	Gas constant – CHANGE
RBC	Relative Battery Capacity
S_e	Share of EV in the car fleet
s_{batt}	Battery size (kWh)
S_{BAU}	Business As Usual (BAU) scenario
S_{MO}	Multi-objective battery dispatch scenario
S_{pax}^{veh}	Share of EA passengers arriving by EV
S_{PS}	Peak shaving scenario (w/o PV)
S_{PS}^{pv}	Peak shaving scenario (w/ PV)
S_{pv}	Reference scenario w/ PV
s_{pv}	PV size (kW)
S_{ref}	Reference scenario
S_{TZ}	Target Zero battery dispatch scenario
SC	Self-consumption
SOC	(Battery) state-of-charge
SOC_{lb}	SOC lower boundary
SOC_{max}	Maximum battery SOC
SOC_{min}	Minimum battery SOC
SS	Self-sufficiency
T	Absolute temperature
TZ	Target Zero battery dispatch algorithm
U_{nom}^{batt}	Battery nominal operating voltage
U_{nom}^{cell}	Cell nominal operating voltage
U_{nom}^{conv}	Converter nominal operating voltage
V2G	Vehicle to grid

Energy Management, where alternative and renewable energy sources, such as solar energy, were categorised as one sub-indicator.

1.2. Related works

Schäfer et al. simulate replacing all global flights up to 600 nautical miles with EA and estimates that this corresponds to an increased energy demand of 112–344 TWh (0.6–1.7% of 2015 global consumption) [8]. From a study of the O'Hare International airport, a portion of the flights are replaced by hybrid electric aircraft and the change in electricity demand was studied [9]. The results conclude that a substantial increase in the energy demand is needed, requiring airport grid upgrades.

Kaya et al. assessed the passengers' airport sustainable design requirements and found that PV installation was their top priority [6]. In an assessment of the PV potential for Chinese civil airports, the combined PV power capacity of the 239 airports amounted to 2.5 GW/a with a total generation of 2.65 TWh [10]. The referred study also quantifies the self-sufficiency (SS) potential of PV and concludes that for 23 out of 31 provinces, the SS rate is more than 50%. Furthermore, the study concludes the need for electrical storage to mitigate the intra-day mismatch between load demand and PV generation. Sukumaran et al. evaluate the performance of a 12 MW PV installation at the Cochin International airport in India and conclude that PV deployment effectively reduces the airport's economic and environmental footprint [11]. Baek et al. determine the optimal PV sizes for Incheon International Airport, South Korea, for a reference load demand and two load-expansion scenarios: 120 and 140% of the Ref. [12]. The study

concludes that PV can cover the predicted load expansions. Baxter et al. examined the effect of the PV installation at Adelaide Airport, Australia and found tangible gains; 10% year-to-year reduced energy consumption [13]. The advantages of PV airport deployment are also highlighted in, e.g., [14,15]. However, the benefits of including PV depend on the timely correlation with load demand. Including stationary battery energy storage system (BESS) could further enhance the benefits by reducing grid energy demand, electricity cost, and access to renewable energy.

Micallef et al. [16] reviewed the concept and potential for microgrids and acknowledged that the airport's cross-sector coupling could benefit from a microgrid implementation. The refereed study also concludes that airports are the least explored transport-related sector addressing the microgrid concept and the electrification challenge. The lack of microgrid studies of airports are also acknowledged in [17,18]. In [17], the effect of vehicle-to-grid (V2G) and EA charging strategies are studied for an airport micro grid with PV and hydrogen storage. Xing et al. use a mixed integer linear programming (MILP) optimisation to compare the techno-economic performance of five airport energy configuration systems, including combinations of PV, BESS and hydrogen storage [14]. The study excludes EA but concludes cost and emission savings when implementing PV and storage by reducing electricity from the grid. Alruwaili et al. use a modified MILP to evaluate the techno-economic potential of an airport microgrid with PV, BESS and a backup diesel generator [19]. The MILP minimises operation costs and enhances the airport's power resilience. Similar to [14,19], Zhao et al. use a MILP based on life cycle theory to evaluate an airport's techno-economic feasibility and resilience, excluding the electricity usage at the terminals [20]. Typical for the reviewed studies on airport micro grid operation is the use of a single-objective storage (BESS and hydrogen) dispatch to maximise self-consumption (SC) from the PV generation [14,17]. Trainelli et al. model the optimal airport battery sizing to support EA charging (single-objective) and acknowledge the potential of revenue-stacking operation [21]. Examples of operational shortcomings of BESS single-objective operation are shown practically in [22] and through simulations in [23]. In both cases, the results highlight the poorly managed operation when relying solely on PV surplus. As identified in [24–27], single-objective operation limits the BESS's full potential thus leaves out technical and economic possibilities.

This work taps into the research gaps in the literature by addressing: (i) holistic airport micro grid modelling, including EA, EV, PV and BESS, (ii) exploring the techno-economic effect of varying BESS operations, and (iii) presenting a novel revenue-stacking multi-objective (MO) battery dispatch operation. The examined case is a high-latitude airport with significant energy and power demand increase from EA and EV charging.

1.3. Aim and contributions from this work

This work addresses the increased demand for electricity at an airport, driven by the societal electrification trend, particularly in the transport sector from EA and EV. It fills the current research gap by examining the role of PV and stationary BESS using different dispatch algorithms and quantifies their respective effect from a techno-economic perspective. A novel revenue-stacking MO battery dispatch is presented, optimising the BESS operation by combining self-consumption enhancement and peak power shaving. The economic evaluation includes the monetised battery degradation, hourly electricity grid trade and peak power tariff. In summary, this work provides insights into the potential benefits and economic viability of integrating PV and BESS in a Nordic airport and demonstrates how PV and BESS can aid increased electrification. The specific contributions provided in this work are:

- the use of measured airport load demand and realistically modelled EA and EV charging profiles,
- proposed revenue-stacking MO battery dispatch for combined SC and peak shaving operation,
- quantified techno-economic effects from various BESS operation objectives, and,
- quantified BESS degradation and associated cost from varying dispatch operations.

2. Theory

2.1. Battery model

In the simplest of forms, a battery can be represented via the *Rint* model with a series-connected ohmic resistance, R, [28] and an open-circuit voltage (OCV), $u_{OCV}(t)$. The cell's nominal voltage, $u_{batt}(t)$, can be approximated as [29]

$$u_{batt}(t) = u_{OCV}(t) + i_{batt}(t)\mathrm{R} \tag{1}$$

where $i_{batt}(t)$ is the battery current and is defined as negative for discharge and positive for charging. The OCV is a function of the battery's state-of-charge (SOC) and is characterised through experimental measurements [30]. The SOC defines the instantaneously available energy content and is defined as [31]

$$\mathrm{SOC}(t) = \frac{q_{batt}(t)}{\mathrm{Q}_{batt}^{rated}} = \frac{\int i_{batt}(t)dt}{\mathrm{Q}_{batt}^{rated}} \tag{2}$$

where $q_{batt}(t)$ and $\mathrm{Q}_{batt}^{rated}$ are the charge level and rated capacity, respectively.

Assuming cell uniformity, the required number of series-connected battery cells (n_{cell}), rounded to the nearest integer, is given as

$$\mathrm{n}_{cell} = \mathrm{ceil}\left(\frac{\mathrm{U}_{nom}^{conv}}{\mathrm{U}_{nom}^{cell}}\right) \tag{3}$$

where U_{nom}^{conv} and U_{nom}^{cell} are the converter's and battery cell's nominal operating voltages, respectively. Using (3) and the battery cell's nominal capacity, Q_{cell}, the required number of parallel strings ($\mathrm{m}_{strings}$) for a given battery size, E_{batt}, is given as

$$\mathrm{m}_{strings} = \mathrm{ceil}\left(\frac{\mathrm{E}_{batt}}{\mathrm{U}_{nom}^{batt}\mathrm{Q}_{cell}}\right). \tag{4}$$

And using (4), the string current, equal to the current through each series-connected cell, is calculated as

$$i_{cell}(t) = \frac{p_{batt}(t)}{u_{batt}(t)}\frac{1}{\mathrm{m}_{strings}} \tag{5}$$

where $p_{batt}(t)$ and $u_{batt}(t)$ are the battery power and voltage, respectively.

Battery ageing consists of calendar and cycle ageing, where the former depends on time, temperature and SOC, and the latter also on the battery operation, e.g., the number of equivalent cycles, depth of discharge (DoD) and C-rate [32]. Based on the power law equation introduced in [33], the work in [34] developed a cycle degradation model for a graphite-$LiFePO_4$ battery cell. This degradation model considers the operating temperature, time, depth of discharge (DoD) and discharge rate to calculate the cell's capacity fade. Derived from the power law equation, Wang et al. [34] replace the time dependency for capacity throughput (A_h) and define the capacity loss, $q_{loss}(t)$, as

$$q_{loss}(t) = \mathrm{B}\exp\left(\frac{-\mathrm{E}_a}{\mathrm{R}_g\mathrm{T}}\right)A_h(t)^{\mathrm{z}} \tag{6}$$

where R_g is the gas constant, T is the absolute temperature (in K), and z is the power law factor. The pre-exponential factor, B, and the activation energy, E_a, are parameterised from experimental tests for different C-rates and operating temperatures [34]. The capacity throughput (A_h) is calculated as

$$A_h(t) = n(t) \cdot \mathrm{DoD} \cdot \mathrm{Q}_{cell} \tag{7}$$

where $n(t)$ is the cycle number. The degradation model from (6) and (7) is widely used in the literature, e.g., [35–38].

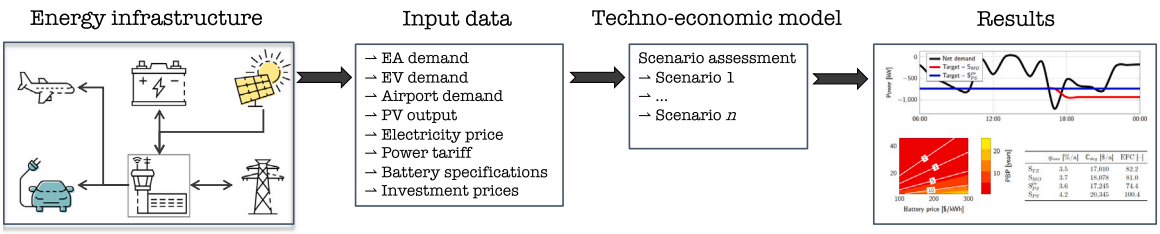

Fig. 1. Modelling procedure outline.

2.2. Self-consumption and self-sufficiency

The quantity of self-consumed electricity from PV generation ($M(t)$) is defined as [39]

$$M(t) = \min\left[L(t);\ P(t) + S(t)\right] \tag{8}$$

where $L(t)$ is the load demand, $P(t)$ is the PV generation, and $S(t)$ the charge and discharge powers. Here, $S(t)$ is defined as positive for discharge and negative for charge. Integrating (8) over time, T, for a system without battery storage gives the share of PV SC as

$$\vartheta_{SC} = \frac{\int^T M(t)dt}{\int^T P(t)dt} \tag{9}$$

where $P(t)$ is the total generated PV energy. This definition is true if there is no interaction between the battery and external grid, that is, no charging or discharging from/to the grid. If the battery is allowed to interact with the grid, (9) can be expanded according to [40] as

$$\vartheta_{SC} = \frac{\int^T M(t)dt - B(t)dt}{\int^T P(t)dt} \tag{10}$$

where $B(t)$ denotes the energy from the grid for charging the battery, the SS is calculated from (9) and (10) by switching from total PV generation in the denominator to total load demand.

3. Method

3.1. Case study: Visby airport

Located in Gotland (Sweden), the only competing transportation to mainland Sweden and neighbouring countries is via ferry. In 2019, before the Covid pandemic, the airport had more than 8000 arriving passengers. The hourly load demand from 2018 is acquired and denoted as 'Business As Usual' (BAU) for this work. A seasonal variation in load demand and PV output is present from the geographical location of the airport. As the electricity demand is dominated by (electric) heating, an apparent seasonal variation in load demand is present. The seasonal load demand and PV availability have a negative correlation, meaning that PVs ability to aid the increased energy and power demands varies throughout the year. Furthermore, the seasonal variation in load demand also present vary peak power demands from the grid.

Fig. 1 outlines the modelling procedure, including the energy infrastructure power flows, input data, scenario analysis and result generation.

3.2. Aircraft charging profiles

A simulation model has been developed to investigate airport power capacity requirements if battery-driven EA is introduced [41]. Electric aircraft are expected to have relatively large batteries that are also likely to be charged within short time intervals at the airports (turnaround times) to enable sufficient range. Thus, the power capacity demand may increase at the airports if several aircraft charge simultaneously. Regarding aircraft technology, the model and its flight simulations are based on an electric aircraft model, parameterised per certification level CS/FAR-23 (19 seats and maximum take-off weight of 8618 kg) [42].

A scenario with 16 EA flights per day and direction has been investigated in this work, capable of transporting 300+ passengers in each direction using a 19-seat aircraft. In 2019, Visby Airport had approximately 219,000 arriving passengers and 214,000 departing passengers [43]; on average, 600 passengers per direction and day. The suggested EA schedule can thus handle 50% of the average daily passenger demand.

As the energy density of batteries is much lower than traditional jet fuel, EA will initially be limited to shorter distances. The EAs are modelled with 800 kWh available battery storage. Flights are simulated for six short-haul domestic EA routes to/from Visby Airport (ESSV) shown in Fig. 2, each within a range of approximately 200 km. These include Stockholm Bromma Airport (ESSB), Stockholm Skavsta Airport (ESKN), Norrköping-Kungsängen Airport (ESSP), Linköping/SAAB Airport (ESSL), Västervik Airport (ESSW), and Kalmar Airport (ESMQ). Only the ESSB connection is a commercial route today, meaning that the rest are new routes that could be served by EA in the future, given the proximity. A flight schedule for these routes is created by setting a desired number of flights in different daily periods per route and direction. For the scenario, the distribution of flights has been designed as a "commuter schedule" with primarily morning and afternoon flights. An optimisation model is then introduced, which generates a schedule where the entire flight demand is met with the minimum number of electric aircraft. As shown in Fig. 3, the 32 flights can be covered under defined periods using four electric aircraft (MF001–MF004). All flights are depicted as diagonal lines between airports and colour-coded per aircraft. Every flight is succeeded with a horizontal line representing turnaround time at the destination airport.

Next, energy consumption is simulated step-by-step, followed by charging simulations during the turnaround. Finally, the six airports' resulting power requirements are summed at every time step. Fig. 4 shows the daily load curve from EA charging at Visby Airport. The EA use independent fast-charging with a SOC dependent power [41,44] as

$$p_{ch}^{EA}(\mathrm{SOC}) = \begin{cases} 2\ \mathrm{C}, & \text{if } 40\% \geq \mathrm{SOC(t)} > 0\% \\ 1\ \mathrm{C}, & \text{if } 80\% \geq \mathrm{SOC(t)} > 40\% \\ 0.5\ \mathrm{C}, & \text{otherwise} \end{cases}$$

3.3. Electric vehicle charging profiles

Charging of EVs at the airport parking is simulated based on flight schedules, assumed parking patterns and other site-specific parameters. It is assumed that the vehicle arrivals are connected to flight departures. The number of EVs arriving before each departure, N_{EV}, is calculated as

$$\mathrm{N}_{EV} = \left(\frac{\mathrm{N}_{seat}^{ac}\,\mathrm{CF}_{ac}\,\mathrm{S}_{pax}^{veh}}{\mathrm{N}_{pax}^{veh}}\right)\mathrm{S}_e \tag{11}$$

where N_{seat}^{ac} is the seating capacity of the departing aircraft, CF_{ac} the aircraft cabin factor, S_{pax}^{veh} the share of flight passengers arriving by car, N_{pax}^{veh} the number of passengers per car (car-sharing), and S_e the share of electric vehicles in the car fleet. Before each departure, N_{EV} arrivals

Fig. 2. Potential short-haul flight connections to/from Visby Airport within a 200 km radius modelled as EA flights.

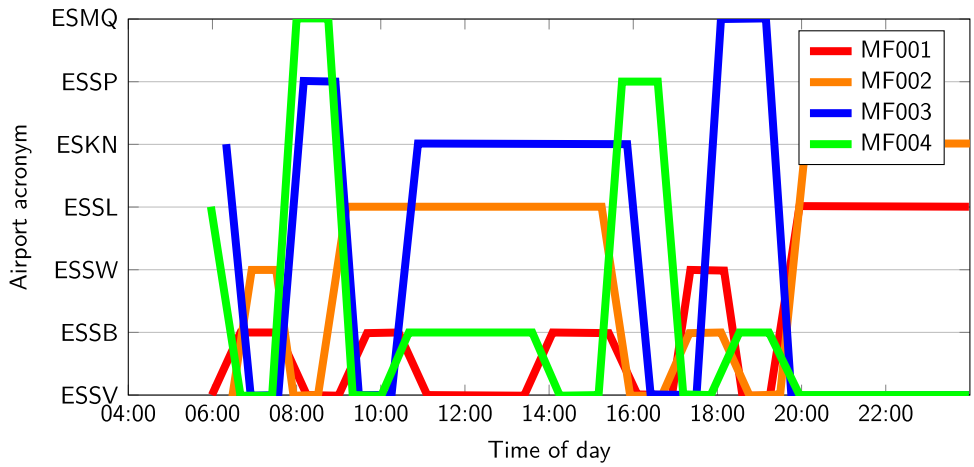

Fig. 3. Representation of the optimised flight schedule. Aircraft movements between airports are shown as coloured lines. Airport acronyms: Visby (ESSV), Stockholm Bromma (ESSB), Västervik (ESSW), Linköping/SAAB (ESSL), Stockholm Skavsta (ESKN), Norrköping-Kungsängen (ESSP) and Kalmar (ESMQ).

are sampled from probability density functions for arrival time (in minutes before the flight departure), parking duration, and battery SOC at arrival. As seen in Fig. 5(a), the average arrival time is 45 minutes before flight departure and parking duration is 1–2 days (Fig. 5(b)), and SOC upon arrival is modelled with a Gaussian distribution around 50%. The flight schedule is defined for a single day, whilst parked EVs might span several days. Considering that the EV charging sessions overlap with earlier days is essential. To capture this effect, the model starts by simulating one set of parking sessions according to the method described above and stores the maximum number of days that any of the vehicles stay parked. The flight schedule is then repeated for that number of days, simulating a new set of EV parking sessions each day and stacking overlapping sessions. Finally, the EV charging profile for the last day is stored, as it best represents the aggregated load for the maximum overlapping sessions. The share of EVs, S_e in (11), is set to 25%. A power limit per charging outlet is 7.4 kW with a 95% efficiency. Consequently, charging is modelled with a constant power of 7.03 kW/EV until fully charged; after that, the EV remains in the parking space.

3.4. Solar photovoltaic design

Airport specifications such as size, location, available space, air traffic activities and weather conditions can significantly affect the solar photovoltaic system design. In this case study, three potential locations were suggested by the airport technical team during a visit to Visby Airport; see Fig. 6. Possible risks to air traffic and aviation system by glare [45] or glint from sun reflection, disturbance of radio communication system and other instruments, and physical obstacles at the airport were considered during the selection procedure [46]. Location 1 is a ground-mounted array system located reasonably far from the airport building and communication tower. Location 2 is the parking space, and PV panels could be installed on the roof. However, it does not have a roof yet. Also, location 2 is relatively close to the Airport Traffic Control Tower (ATCT) with a risk of electromagnetic interference to the communication system [47,48]. These specifications will be used in further evaluation of potential PV system installations at the airport. Location 3 is a ground-mounted array system located south-west of the main airport building.

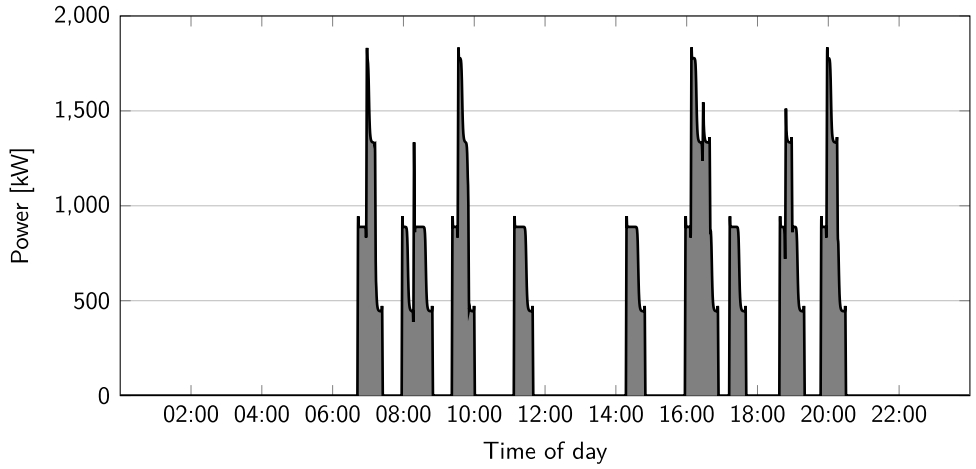

Fig. 4. Daily power demand from EA charging at Visby Airport.

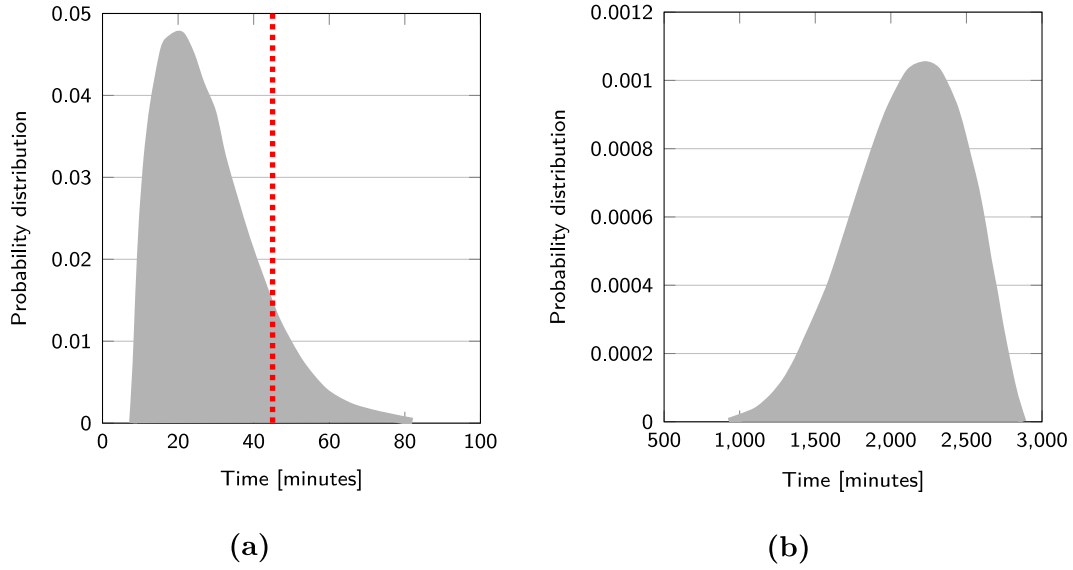

Fig. 5. Probability distribution of **(a)**: passenger car arrival time before flight departure and **(b)**: car parking duration.

Table 1
Solar photovoltaic (PV) module specifications.

Specification	Value
Panel dimensions [m]	1.046 × 1.559
Panel area [m^2]	1.63
Rated power [W]	370

Table 2
Solar array designs and specifications for the modelled locations.

Spatial planning	PV1	PV2	PV3
Array area [m^2]	12,732	6,968	2,880
Number of modules	2,632	3,168	556
Inter-row spacing [m]	4	– (rooftop)	4
Tilt angle[a] [°]	35	5	35
Azimuth angle(s)[a] [°]	180	156, 110 and 21[b]	180

[a] Tilt and azimuth angles are fixed.

[b] Tilt angle distribution: 38 kW at 21°, 164 kW at 110° and 970 kW at 156°.

Table 3
PV array simulation results.

	PV1	PV2	PV3
Total array power [kW]	974	1,172	206
Annual yield [MWh]	1,083	1,125	230
Specific yield [kWh/kWp]	1,112	960	1,116
Performance ratio [%]	82.7	85.3	83.0
Shading loss [%]	4.3	0.1	4.0

3.4.1. PV system simulation

Typical Meteorological Year (TMY), 10 km Grid, Meteonorm weather was used in the HelioScope PV simulation software [49] to acquire the output profiles. The array sizes are determined from the available space to maximise the annual yield. In locations 1 and 3, the panels have a fixed tilt angle of 35°, facing due south (azimuth angle of 180°) and an inter-row spacing of 4 metres. In location 2, the solar panels are on the parking roof with a tilt angle of 5°. In most cases, the azimuth angles are based on the parking orientation, which is 156°. The PV modules and array's technical specifications are shown in Table 1 and Table 2, respectively, and the simulation results are in Table 3.

3.4.2. PV and load demand correlation

From (9), the SC and SS are calculated for the three PV arrays (PVn) and aggregated arrays (PVtot). The results are shown in Fig. 7 for four

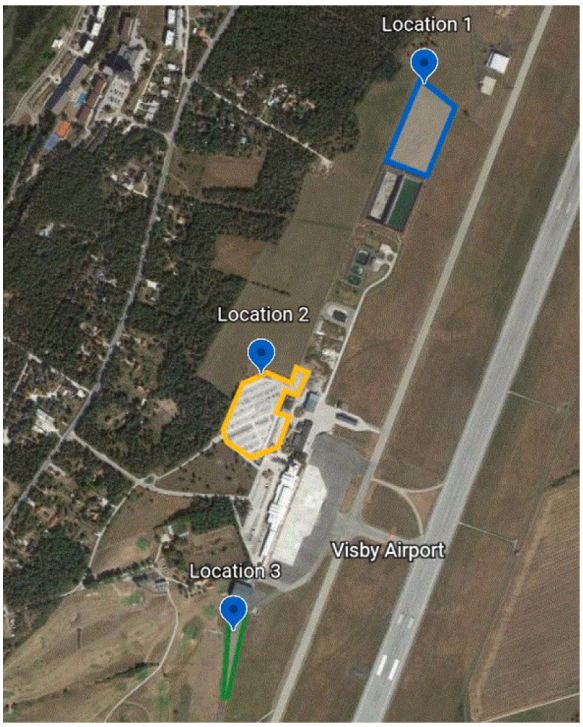

Fig. 6. Potential locations for PV system installation at Visby Airport.

load scenarios: 'All loads' (BAU + EA + EV), BAU, EA, and EV. The load demand directly consumes all energy from PV3 (Fig. 7(a)) in the BAU scenario—and consequently also for 'All loads'—meaning that this array alone is relatively small in comparison to the load demand and further proven by a SS below 10% in Fig. 7(b). Locations 1 and 2 have comparable yields (see Table 3), and despite the variation in azimuth angles, the effect on SC and SS is marginal. For the continuation of this work, PV generation in location 1 (PV1) is chosen considering the similar effect on the technical performance as location 2 and the realisation challenges of location 2 outlined in Section 3.4.

3.5. Target zero battery dispatch

The 'Target Zero' (TZ) algorithm for maximising SC is adopted from [50,51]. The maximum charge and discharge powers, P_{batt}, are constrained by the battery's power electronic converter. In this work (for all battery algorithms), P_{batt} is set to 80% (0.8 C) of the energy capacity. This operation maximises the self-consumed PV and limits grid energy import, with the battery size and SOC range (SOC_{max}–SOC_{min}; 90 and 15%, respectively) limiting the storage capacity.

3.6. Peak power shaving battery dispatch

Other studies in the literature on battery peak shaving typically use a forecast for the net grid interaction, e.g., [52–54]. In the current work, on the other hand, no forecast is used. Instead, the operation is dictated via a rule-based control strategy outlined in Fig. A.15 and peak-shaves to a target value set by the monthly peak power usage. The control uses the available power cap-defined from the difference between the instantaneous net demand and target value—to charge from the grid ($p_{net}(t)$) to ensure sufficient SOC. Compared to the TZ algorithm, the peak shaving algorithm uses an expanded DoD (85%) by lowering the minimum SOC limit to 5% (SOC_{lb}). Peak shaving $p_{sh}(t)$ occurs whenever the instantaneous net demand exceeds the current monthly target. After each time step, the target value is compared to the grid import; if the import exceeds the target, a new target value is set. The power tariff is based on monthly performance and reset to zero at the start of the month. The peak shaving algorithm is modelled with (S^{pv}_{PS}) and without PV generation (S_{PS}), and the operation without PV is shown in Fig. A.16.

Table 4
Scenario modelling matrix.

	S_{BAU}	S_{ref}	S_{pv}	S_{TZ}	S_{MO}	S^{pv}_{PS}	S_{PS}
Reference load demand	✓	✓	✓	✓	✓	✓	✓
Electric Aviation		✓	✓	✓	✓	✓	✓
Electric Vehicle		✓	✓	✓	✓	✓	✓
Solar photovoltaic			✓	✓	✓	✓	
Battery storage				✓[a]	✓[b]	✓[c]	✓[d]

[a] Battery control from [50].
[b] Battery control: Figs. A.17 and A.18.
[c] Battery control: Fig. A.15.
[d] Battery control: Fig. A.16.

3.7. Multi-objective battery dispatch

The proposed MO combines the two objectives from Sections Section 3.5 (maximised SC) and 3.6 (peak shaving) in a rule-based operation. The operation is described in Fig. A.17. The κ term ensures that: (i) grid power is not used to charge the battery entirely (C_3), and (ii) grid-charged energy is not used for discharge to cover the load demand (C_4). The MO include a seasonal variation of the minimum SOC level, $soc^{su}_{min}(t)$, outlined in Fig. A.18. Here, $soc^{su}_{min}(t)$ is constrained by SOC_{lb} and SOC_{max} from Fig. A.17: $SOC_{lb} \leq soc^{su}_{min}(t) \leq SOC_{max}$. Similar with the peak shaving in Figs. A.15 and A.16, the DoD is defined between SOC_{lb} and SOC_{max}. The SOC variation in Fig. A.18 is dictated by the PV export ($pv_{exp}(t)$) from the previous 24 h (dt). If PV is exported, $soc^{su}_{min}(t)$ reduces by δ_{soc}, and if no export is done, $soc^{su}_{min}(t)$ increases by δ_{soc}. This work uses a δ_{soc} of 5% if not mentioned otherwise. The minimum SOC level thus has a clear seasonal variation depending on the preceding day's operation and the presence of PV export.

3.8. Airport energy system scenarios

Four main scenarios are modelled and evaluated, with one scenario divided into four sub-scenarios. The scenarios, S_x, are:

- **S_{BAU}** – represents today's situation and uses the measured load demand from Section 3.1.
- S_{BAU} with added EA (Section 3.2) and EV (Section 3.3) profiles. This case quantifies the added grid stress and energy demand from EA and EV and denotes the reference in the foreseen future scenario; **S_{ref}**.
- Scenario **S_{pv}**; added PV generation (see Section 3.4) to the reference case, S_{ref}.
- Added BESS to S_{ref} with four types of control algorithms:
  - **S_{TZ}** – S_{pv} with battery dispatch from Section 3.5.
  - **S_{MO}** – S_{pv} with multi-objective (MO) battery dispatch from Section 3.7.
  - **S^{pv}_{PS}** – peak shaving algorithm with PV generation; see Section 3.6 and Fig. A.15.
  - **S_{PS}** – peak shaving without PV; see Fig. A.16.

The results from the battery scenarios quantify, on the one hand, the effect of BESS and, on the other hand, the effect of the chosen battery dispatch algorithm. Table 4 summarises the scenarios.

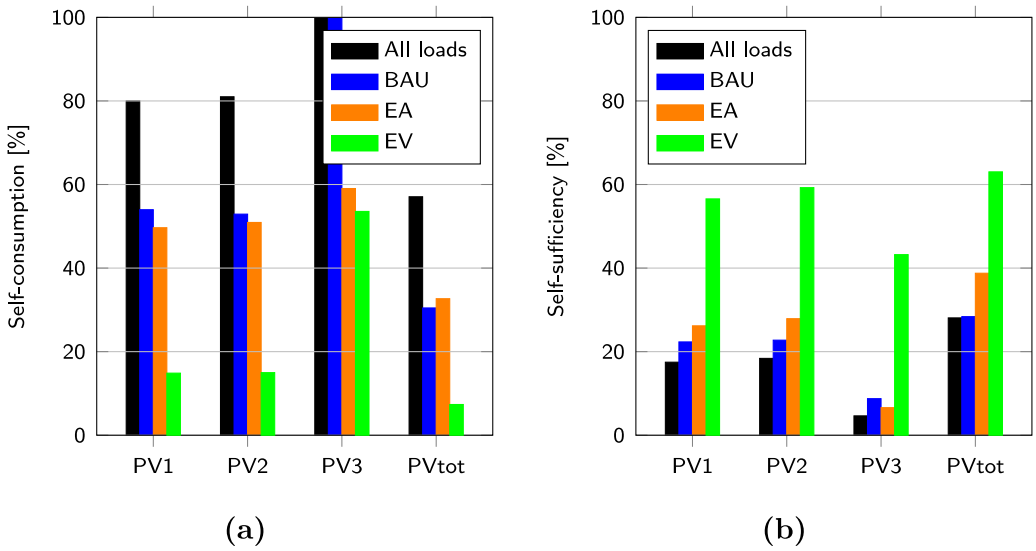

Fig. 7. PV self-consumption **(a)** and self-sufficiency **(b)** for the PV arrays and load scenarios.

Table 5
Technical specifications of the modelled battery pack [57].

	Value	Comment		Value	Comment
Q_{cell}	12 Ah	[57]	R	3 mΩ	R per n_{cell} in (1)
U^{cell}_{nom}	3.2 V	[57]	n_{cell}	250	See (3)
U^{batt}_{nom}	800 V		$m_{strings}$	227	See (4)

3.9. Battery sizing and design

The modelled battery size is derived from the Relative Battery Capacity (RBC) index and a method applied for residential buildings in Sweden [55] as a function of PV array nominal power as

$$\text{RBC} = \frac{E_{batt}}{E_{PV}} \tag{12}$$

where E_{batt} is the battery's energy capacity and E_{PV} the annual PV yield. In the referred study, the PV array size is modelled as a function of annual load, defined from a study on high-latitude PV systems [56], as

$$\text{ALR} = \frac{P_{PV}}{P^{avg}_{load}} \tag{13}$$

where P_{PV} is the PV array peak power (Wp) and P^{avg}_{load} the annual average load demand. Using the two load demand scenarios from Section 3.8, the ALRs in (13) are 1.7 and 3.2, with and without the EA and EV demands, respectively.

As concluded in previous works, e.g., [40,55], the effect of increased battery size on the SC diminishes at a certain point, resulting in poor utilisation for larger sizes. Fig. 8 shows SC as a function of battery size (E_{batt}) and RBC for scenario S_{TZ} (ALR = 1.7). Marginal improvements in SC are observed for RBC>2. Thus, to optimise the BESS for SC enhancements while maintaining good utilisation, an RBC = 2 is used in (12), resulting in an energy capacity, E_{batt}, of 2.2 MWh, and used for all scenarios in Table 4.

The nominal battery voltage (U^{batt}_{nom}) is set to 800 Vdc, and the technical specification and resulting parameters using (3) and (4) are given in Table 5. The modelled battery voltage and current characteristic is validated in [30].

3.10. Economic evaluation

Using the Nordic spot electricity price, $\mathbb{C}_{NS}$, the hourly price for bought electricity is, in this work, calculated as

$$\mathbb{C}_{bought}(t) = \left(\mathbb{C}_{NS}(t) + \mathbb{C}_{tax} + \mathbb{C}_{var} + \mathbb{C}_{cert} + \mathbb{C}_{sur}\right) \tag{14}$$

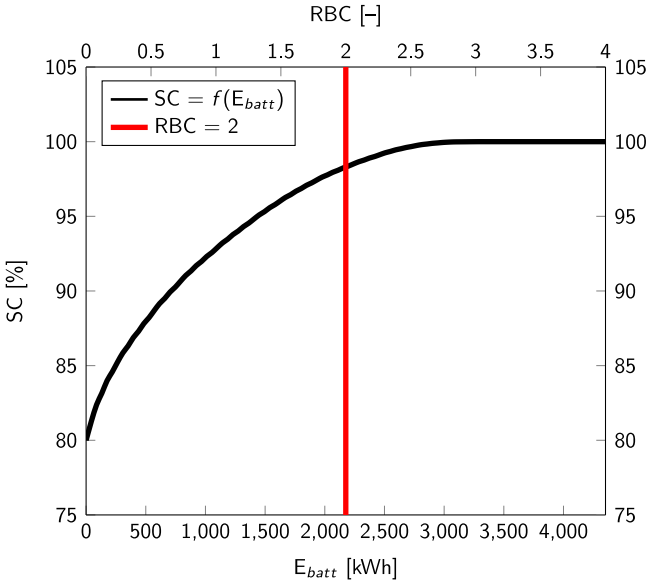

Fig. 8. Self-consumption as a function of battery size (E_{batt}) and RBC for scenario S_{TZ} (ALR = 1.7). The vertical line shows the modelled size in this work (2.2 MWh/RBC = 2).

where $\mathbb{C}_{var}$ is the variable grid charge, $\mathbb{C}_{cert}$ the price of bought electricity certificates, $\mathbb{C}_{sur}$ electricity surcharge, all with a VAT of 25%. The revenue from sold electricity is set equal to the hourly spot price, $\mathbb{C}_{NS}(t)$, as

$$\mathbb{C}_{sold}(t) = \mathbb{C}_{NS}(t) \tag{15}$$

where $\mathbb{C}_{NS}(t)$ are retrieved from Nord Pool [58]. Fig. 9 shows the annual hourly variation in bought ($\mathbb{C}_{bought}(t)$) and sold ($\mathbb{C}_{sold}(t)$) electricity in 2018 for SE3 in Sweden. The net electricity bill is thus calculated from (14) and (15) as

$$\mathbb{C}_{net}(t) = \sum^{T} \mathbb{C}_{bought}(t) - \sum^{T} \mathbb{C}_{sold}(t) \quad t \in T. \tag{16}$$

For peak shaving, the cash inflow is defined from the annual savings relative to a reference case, S_{ref}, and calculated as

$$\mathbb{C}_{peak} = \left[\sum_{m=1}^{M} \max(p^m_{S_{ref}}) - \sum_{m=1}^{M} \max(p^m_{Sx})\right] \mathbb{C}_t \tag{17}$$

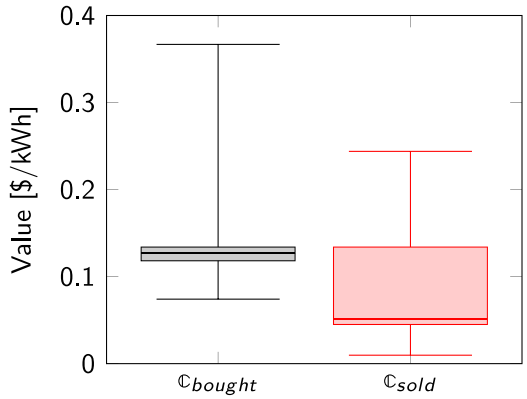

Fig. 9. Hourly variation of bought ($\mathbb{C}_{bought}$) and sold ($\mathbb{C}_{sold}$) electricity in SE3, Sweden from 2018.

where $\max(p^m_{Sx})$ is the monthly peak power imports for month m and scenario S_x, and $\mathbb{C}_t$ the peak power tariff ($/kW).

The economic payback period (PBP) is defined as the required time for the initial investment, I_0, to break even, giving the annual net cash flow. The PBP is calculated using (16) and (17) as

$$\text{PBP} = \frac{I_0}{\sum \mathbb{C}_{peak} + \Delta\mathbb{C}_{net}(t)} \tag{18}$$

where $\Delta\mathbb{C}_{net}(t)$ is the difference in annual electricity bill from the reference case (S_{ref}), with positive values for net annual savings for case S_x. In this work, the initial investment, I_0, is the sum of the PV array and battery storage (when relevant), and calculated as

$$I_0^{PV} = s_{pv} \cdot \mathbb{C}_{pv} \tag{19}$$

$$I_0^{batt} = s_{batt} \cdot \mathbb{C}_{batt} \tag{20}$$

where s_{pv} and s_{batt} are the PV and battery sizes, respectively, and $\mathbb{C}_{pv}$ and $\mathbb{C}_{batt}$ the relative prices (in $/kW and $/kWh). The nominal PV and battery prices are set to 0.635 $/W [59] and 223 $/kWh [60], respectively.

The battery degradation, $q_{loss}(t)$ from (6), impose a cost of usage calculated from the initial investment, I_0^{batt}, as [61,62]

$$\mathbb{C}_{deg} = I_0^{batt} \int^T q_{loss}(t)\text{d}t \quad t \in T. \tag{21}$$

This approach is commonly used in the literature, e.g., [63,64], with a constant $\mathbb{C}_{deg}$ throughout the BESS life time. Unlike previous works with embedded battery degradation models, e.g., [65–67], this work performs a post-process comparison of the battery degradation. Apart from the DoD, the degradation is not considered for in the BESS operations.

4. Results

For the scenarios outlined in Section 3.8, the PV SC and peak power shaving are examined as a consequence of battery control (when applicable). The financial parameters from Section 3.10 are modelled with varying battery prices and peak power tariff charges to examine the investments' economic feasibility. Furthermore, the effect of battery control on annual degradation is examined.

Table 6 summarises the studied cases' power flow analysis results. The addition of EA and EV (S_{ref}) almost doubles the energy demand (+ 89.4%) from today's situation (S_{BAU}) and with an annual peak power increase of more than 1 MW. Without the addition of PV, the energy demand increase is directly reflected in the import demand. Adding PV (S_{pv}) partly covers (17.5%) the increased import but barely affects the peak demand. Scenario S_{PS} relies solely on battery charging from the grid and thus increases the energy import (+ 0.5%) but shaves the peak power demand (−533 kW). The inclusion of storage and dispatch to maximise SC (S_{TZ}–S_{MO}) partly cover the increased load demand (21.5 and 19.4%, respectively). S_{TZ} does little to the peak demand, while S_{MO} gives a significant reduction (−574 kW). S^{pv}_{PS} operation for sole peak shaving barely affects the SC relative to S_{pv} but shaves the peak demand per S_{MO}.

Table 6
Result summary of the power flow analyses for the studied cases.

	S_{BAU}	S_{ref}	S_{pv}	S_{TZ}	S_{MO}	S^{pv}_{PS}	S_{PS}
Load demand [MWh/a]	2,629	4,979	4,979	4,979	4,979	4,979	4,979
Energy import [MWh/a]	2,629	4,979	4,108	3,929	4,019	4,107	5,003
Peak import [kW]	749	1,766	1,707	1,707	1,192	1,192	1,233
PV SC [%]	–	–	80.0	98.3	88.6	80.4	–

Table 7
Annual BESS degradation, monetised degradation cost and equivalent full cycles (EFCs) for the dispatch algorithms.

	q_{loss} [%/a]	$\mathbb{C}_{deg}$ [$/a]	EFC [–]
S_{TZ}	3.5	17,010	82.2
S_{MO}	3.7	18,078	81.0
S^{pv}_{PS}	3.6	17,245	74.4
S_{PS}	4.2	20,345	100.4

Fig. 10 shows the monthly peak power imports for the scenarios (excluding S_{BAU}). The addition of PV (S_{pv}) shave peaks in April–September but is merely a consequence of the coincidence of peak demand and PV generation. The coincidental peak shaving also applies when adding battery storage operating with an SC objective (S_{TZ}). For the peak shaving algorithms (S_{MO}–S_{PS}), the operations—first and foremost—result in significantly lower peaks throughout the year. Relative to S_{ref}, the annually aggregated monthly peak shaving for S_{TZ}–S_{PS} are 0.50, 0.52, 6.20, 6.24, and 6.61 MW/a, respectively.

The proposed MO dispatch performs well compared to S^{pv}_{PS} and S_{PS} except for July and September. The discrepancy in September is explained in Fig. 11 showing a comparison between S_{MO} and S^{pv}_{PS} from September 22nd. Fig. 11(a) shows the net demand (PV-Load) and respective power targets, Fig. 11(b) the charge (positive) and peak shavings (negative), and Fig. 11(c) the battery SOCs. Both manage to shave the initial peak at 10 AM (Fig. 11(a)) and afterwards use the grid to charge until the minimum SOC level (Fig. 11(c)). At 5 PM, another peak occurs and is fully shaved by S^{pv}_{PS} but only partially for S_{MO} (−300 kW), generating a new target value for the latter. The difference in SOC explains the discrepancy in performance (Fig. 11(c)), where S^{pv}_{PS} strives to keep it at maximum (90%) throughout. In contrast, the seasonal variation outlined in Fig. A.18 dictates the minimum level for S_{MO}. As the preceding days have exported PV to the grid, the minimum SOC is low to allow for PV storage. At 6 PM, the grid is again used to charge the batteries, and the difference in the cap—defined by the difference between target and net demand—allows S_{MO} to charge with a higher power; see Fig. 11(b).

4.1. Effect of battery dispatch algorithm on battery ageing

Using (6) and (7), the stationary battery degradation from the annual operation is calculated and shown in Fig. 12. As the degradation is a function of energy throughput as per (6), the degradation from S_{TZ} is marginal in the period later October to mid-February, as this control relies on PV surplus for charging. Table 7 show the annual degradation (q_{loss}), monetised degradation cost ($\mathbb{C}_{deg}$), and the number of equivalent full cycles (EFCs) for each battery dispatch algorithm. Analysing the trend between EFCs and degradation demonstrates the effect of DoD on degradation. Despite having the second most EFCs, S_{TZ} operation (DoD = 75%) results in the lowest degradation.

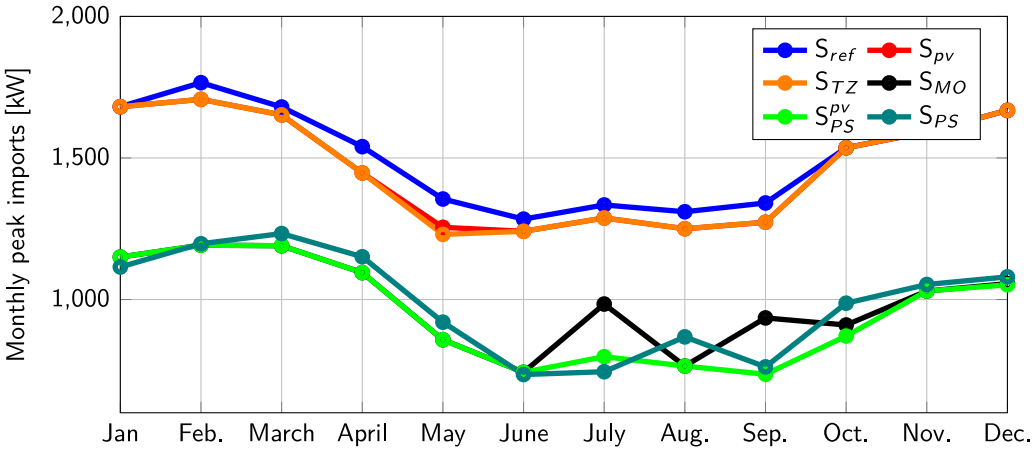

Fig. 10. Monthly peak power imports per scenario S_{ref}–S_{Dn}.

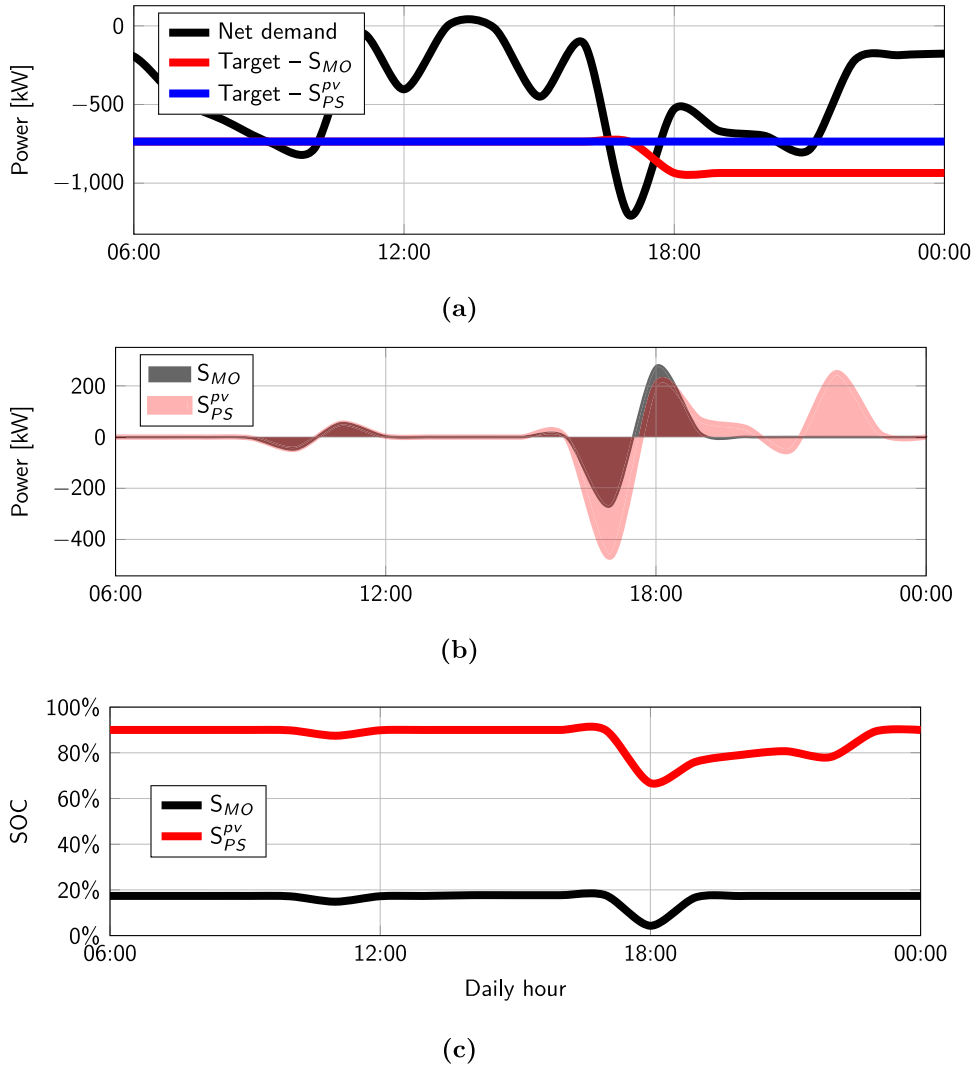

Fig. 11. Working principle of battery storage for S_{MO} and S^{pv}_{PS} from September 22nd showing: **(a)** net demand (PV-Load) and respective power targets, **(b)** battery charge (positive) and peak shaving (negative), and **(c)** battery SOCs.

4.2. Economic assessment of PV and battery investment

Using (14)–(20) enables an economic assessment of the feasibility of PV and battery investments for the assumed billing structure and investment prices in Section 3.10. As aforementioned, the positive cash flow is calculated relative to S_{ref}. Fig. 13 shows the PBP for S_{pv}–S_{PS}. For the nominal economic assumptions, the following results are observed:

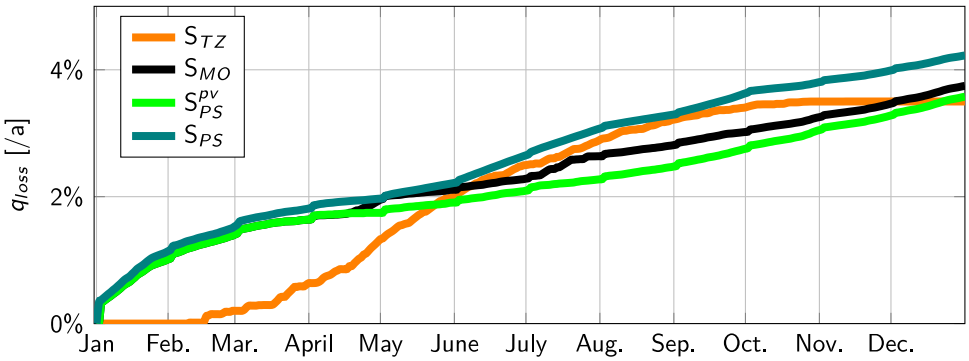

Fig. 12. Annual stationary battery cycle degradation.

- For all cases, the reduction in energy import is the primary source of positive cash flow and determined from the hourly electricity pricing and self-consumed PV energy.
- The scenario without battery storage, S_{pv}, has the lowest PBP of 4.8 years, with 98.2% of the savings from SC.
- For the battery scenarios with PV (S_{TZ}–S^{pv}_{PS}), the proposed rule-based multi-objective dispatch (S_{MO}) has the lowest PBP. For the battery cases, the relative monetary savings share from peak shaving are 1.7, 17.8, and 19.6%, respectively.
- As S_{PS} relies on grid charging of the battery, the electricity bill is higher than for S_{ref} (+ 3404 $/a), and with monetary savings from peak shaving of 28,704 $/a. Considering that the degradation cost from Table 7 is comparable with the net savings (25,300 $/a), the investment is questionable from an economic point-of-view.

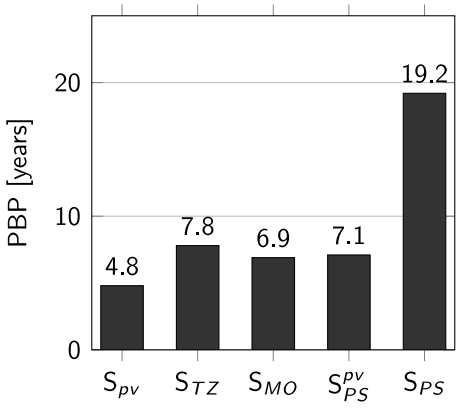

Fig. 13. Payback period (PBP) using the nominal economic assumptions.

A sensitivity analysis of the PBP is made by varying the battery price, $I_0^{batt} \in$ 100–300 $/kWh, and peak tariff, $\mathbb{C}_t \in$ 4.6–46 $/kW. Fig. 14 shows the PBP for the nominal battery size, the battery price ranges, and peak power tariffs. For S_{TZ} (Fig. 14(a)), the battery price has a more significant effect on the PBP than the peak power tariff, seen from the steep PBP slope. This relation comes from the fact above that most of the positive cash flow (98.3%) comes from reduced energy import. As S_{MO} and S^{pv}_{PS} (Figs. 14(b) and 14(c), respectively) have a larger relative share of peak shaving monetary savings (17.8 and 19.6%, respectively), these two are more sensitive to the peak power tariff as seen from the flatter PBP slope. Without PV, the positive cash flow for S_{PS} relies entirely on the peak power tariff. With the nominal economic assumptions, the PBP for S_{PS} is the highest among the battery scenarios; see Fig. 13. However, as seen in Fig. 14(d), the PBP is very sensitive to the peak power tariff. As an example, doubling $\mathbb{C}_t$ more than halves the PBP.

5. Discussion

This work focuses on two battery services: increased SC and peak power shaving. Market arbitrage and power balancing services are examples of other revenue-stacking battery services. Today's intra-day price in the Northern electricity spot market fluctuations incentivises the former. However, as the resilience requirements for airports are outermost important—and hard to monetise—enabling the battery for other services that might interfere with its primary purpose is questionable for this application.

Another way to increase SC and peak shaving is to adjust the PV array tilts and orientations. The PV array design can be adjusted to enhance the supply and demand correlation if the daily load curves are known. This case study has clear power peaks from EA and EV charging in the morning and afternoon. With east–west orientated arrays, these better match the load demand and possibly exclude the necessity for battery storage. An example of load-adapted PV design is presented in [68]. A suggestion for future work is to apply this methodology and examine how this affects the need for battery storage.

For the peak shaving scenarios (S^{pv}_{PS} and S_{PS}), the SOC remains high throughout the year; 90% for more than 78 and 73% of the year, respectively, and with average SOCs for the respective scenarios at 18.8, 73.2, 87.7, and 87.3%. The effect of operating SOC on battery degradation has been investigated experimentally in [69], concluding that higher SOC operation deteriorates the battery faster. Furthermore, [70] reports on the negative correlation of DoD and cycle life. Using the results from this work and the findings in [69,70] suggest that S^{pv}_{PS} and S_{PS} would generate even higher relative degradation.

The simulation model is developed using well-established theoretical models and benchmarks, and the present study provides valuable insights into PV and BESS in the applied case of an airport micro grid. However, future research should address the need for incorporating actual data and hardware to validate further and enhance the reliability and applicability of the approach.

The proposed MO dispatch should be further explored. One suggestion is altering the δ_{soc} (±5% in this work). As seen from the example in September, the lack of available battery capacity was insufficient to shave the peak. Allowing a more significant δ_{soc} variation could benefit a greater peak shaving ability. Furthermore, the inclusion of net demand forecasting should be examined. A rolling target value striving to maintain a specific target could lead to the creation of a greater value without the use of a forecast. Given the repetitive—or, to some extent, pre-known-load demand, a persistent forecast could be sufficient. Alternatively, a pre-defined target value for each month could result in better peak shaving by avoiding the lower peaks.

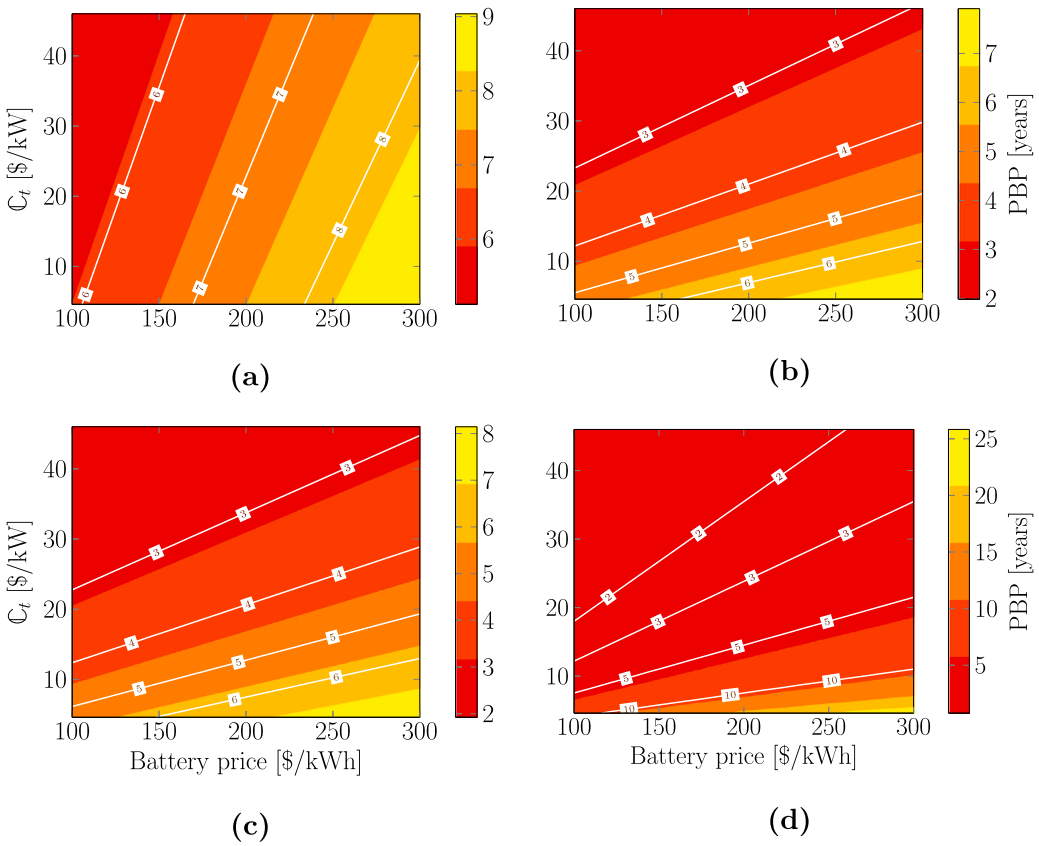

Fig. 14. PBP for: **(a)** S_{TZ}, **(b)** S_{MO}, **(c)** S^{pv}_{PS}, and **(d)** S_{PS}, with varying battery prices (I^{batt}_0) and peak power tariffs ($\mathbb{C}_t$).

6. Conclusions

This work includes a holistic analysis of the airport's energy system in a scenario with a substantial increase in energy and power demands from EA and EV. The techno-economic performance examines the roles of PV and BESS in aiding increased electrification. Furthermore, the effect of inclusion and varying operational objectives of the BESS is compared and quantified, including the effect on battery degradation.

Regardless of the assumptions made for EA and EV charging, these additions substantially increase energy demand and—perhaps more critically—peak power needs. This work demonstrates and quantifies these effects for Visby Airport in Sweden and the potential gains from on-site PV generation and BESS. Specifically, the PV SC and peak power shaving abilities are examined for the studied scenarios, and each scenario's economic feasibility is evaluated.

The results show that substituting the short-haul flights with EA increases the annual load demand by 89.4% and the annual peak power demand by 1 MW. With only PV, the grid demand reduces by 871 MWh through SC (80.0%). The peak reduction, however, is modest and a consequence of the coincidence of PV output and peak power demand. Including BESS further reduce the grid demand from increased SC, up to 18.3 percentage points for S_{TZ} compared to scenario S_{pv}. The SC depends on the battery control algorithm. For the proposed MO dispatch, the SC is 88.6%, that is, 9.7 percentage points lower than S_{TZ}. However, S_{MO} also includes peak-shaving, and the aggregated annual month-by-month peak reduction is 6.2 MW. This peak shaving ability is competitive to sole peak shaving operation (with PV), where scenario S^{pv}_{PS} annually reduces the peak by 6.24 MW/a. A scenario with only battery storage operating for peak shaving shows that the annual peak reduction is 6.61 MW.

An economic evaluation of the PBP for the PV and battery investments demonstrates the sensitivity of battery prices and peak power tariff charges. For S_{TZ}, relying on the reduced demand of bought electricity (through SC), the battery price affects the PBP more. While for the other battery operations, the peak tariff significantly influences the PBP, especially for S_{PS}, which solely relies on peak shaving without PV.

The proposed rule-based multi-objective battery dispatch (S_{MO}) performs well, considering both SC enhancement and peak shaving. Relative to S_{pv}, it enhances the SC with 8.6 percentage points and sufficiently shaves the power peaks. Given the nominal economic assumptions, this operation has the lowest PBP (6.9 years) among the battery scenarios. The MO operation also reduces the battery's idle period, resulting in an annual degradation (3.7%/a) in the same order of magnitude as the other dispatch algorithms (3.5–4.2%/a).

CRediT authorship contribution statement

Patrik Ollas: Writing – review & editing, Writing – original draft, Visualization, Validation, Software, Resources, Methodology, Investigation, Funding acquisition, Formal analysis, Data curation, Conceptualization. **Sara Ghaem Sigarchian:** Writing – review & editing, Writing – original draft, Software, Resources, Methodology, Investigation, Data curation, Conceptualization. **Hampus Alfredsson:** Writing – review & editing, Writing – original draft, Validation, Software, Resources, Methodology, Investigation, Funding acquisition, Formal analysis, Data curation, Conceptualization. **Jennifer Leijon:** Writing – review & editing, Investigation, Funding acquisition, Conceptualization. **Jessica Santos Döhler:** Writing – review & editing, Investigation, Data curation. **Christoffer Aalhuizen:** Writing – review & editing, Investigation, Data curation. **Torbjörn Thiringer:** Writing –

review & editing, Supervision. **Karin Thomas:** Supervision, Project administration, Investigation, Funding acquisition, Conceptualization.

Declaration of competing interest

The authors declare that they have no known competing financial interests or personal relationships that could have appeared to influence the work reported in this paper.

Data availability

The authors do not have permission to share data.

Acknowledgement

The Swedish Energy Agency financially supported the work (Grant No's. 52433-1, 50986-1 and P2022-01305). The authors would also like to thank Swedavia for collaborating on sharing data and discussing feasible system configurations.

Appendix. Battery control flow-charts

See Figs. A.15–A.18.

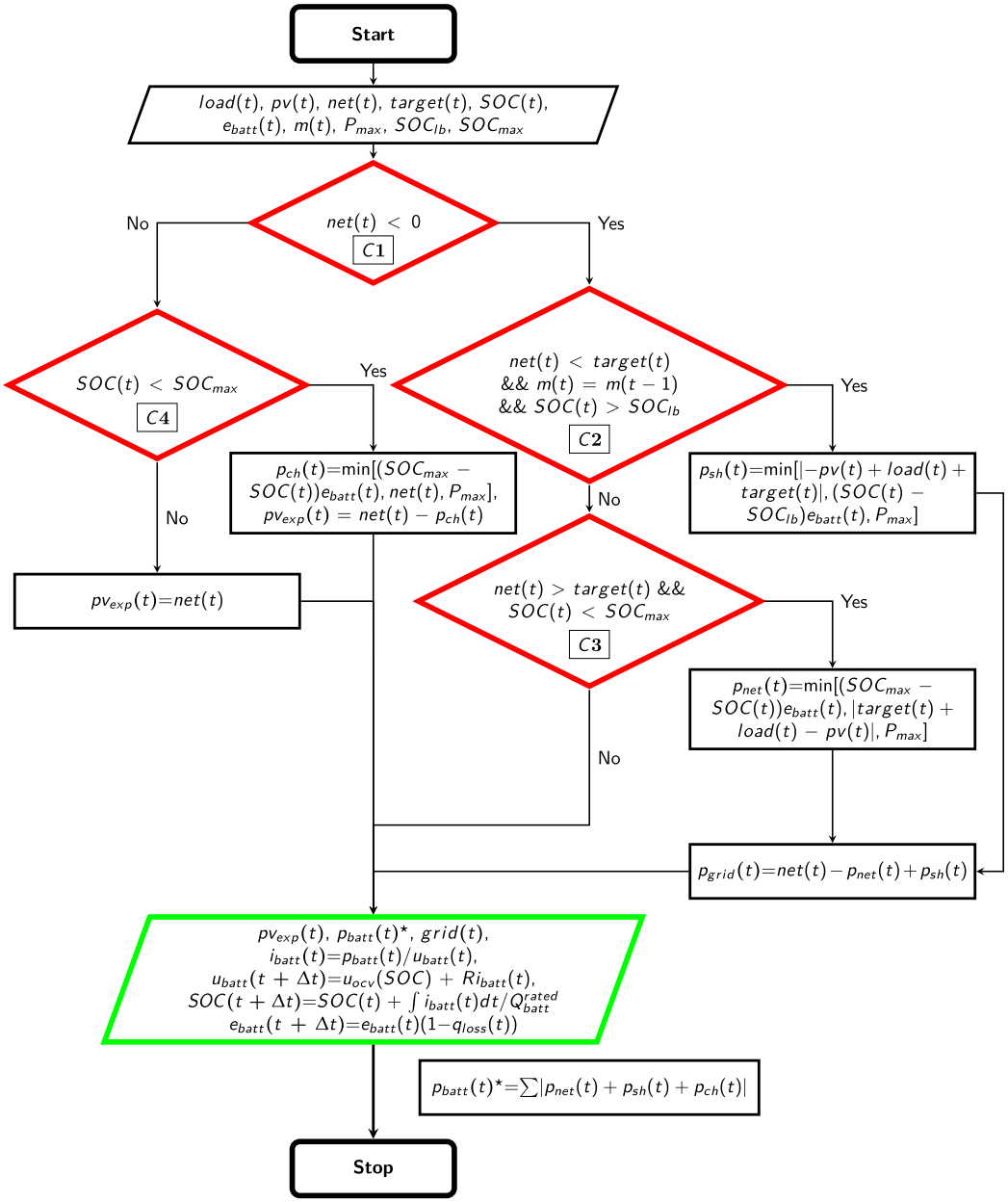

Fig. A.15. Flow chart of battery charge and discharge control for peak-shaving with PV.

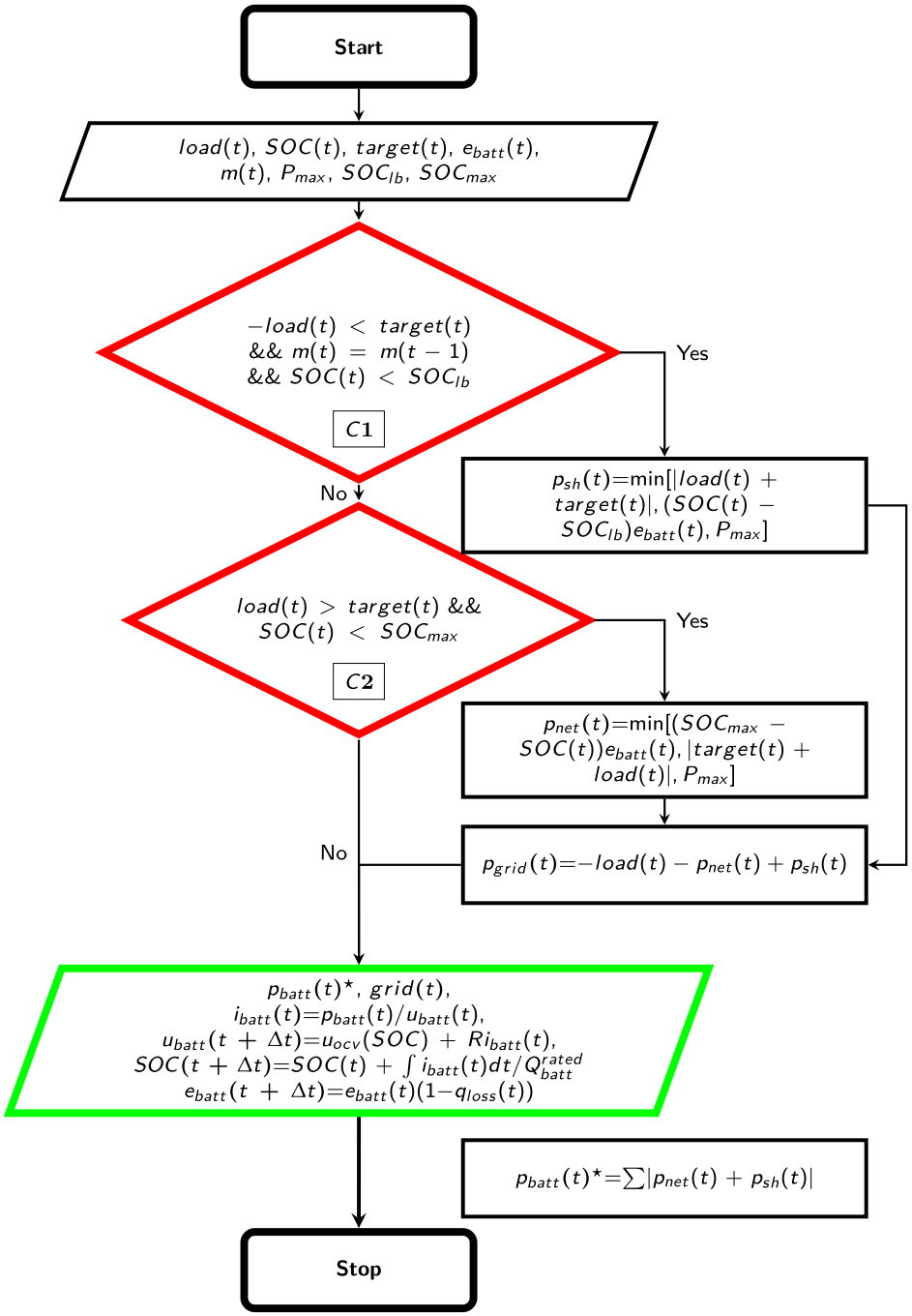

Fig. A.16. Flow chart of battery charge and discharge control for peak-shaving without PV.

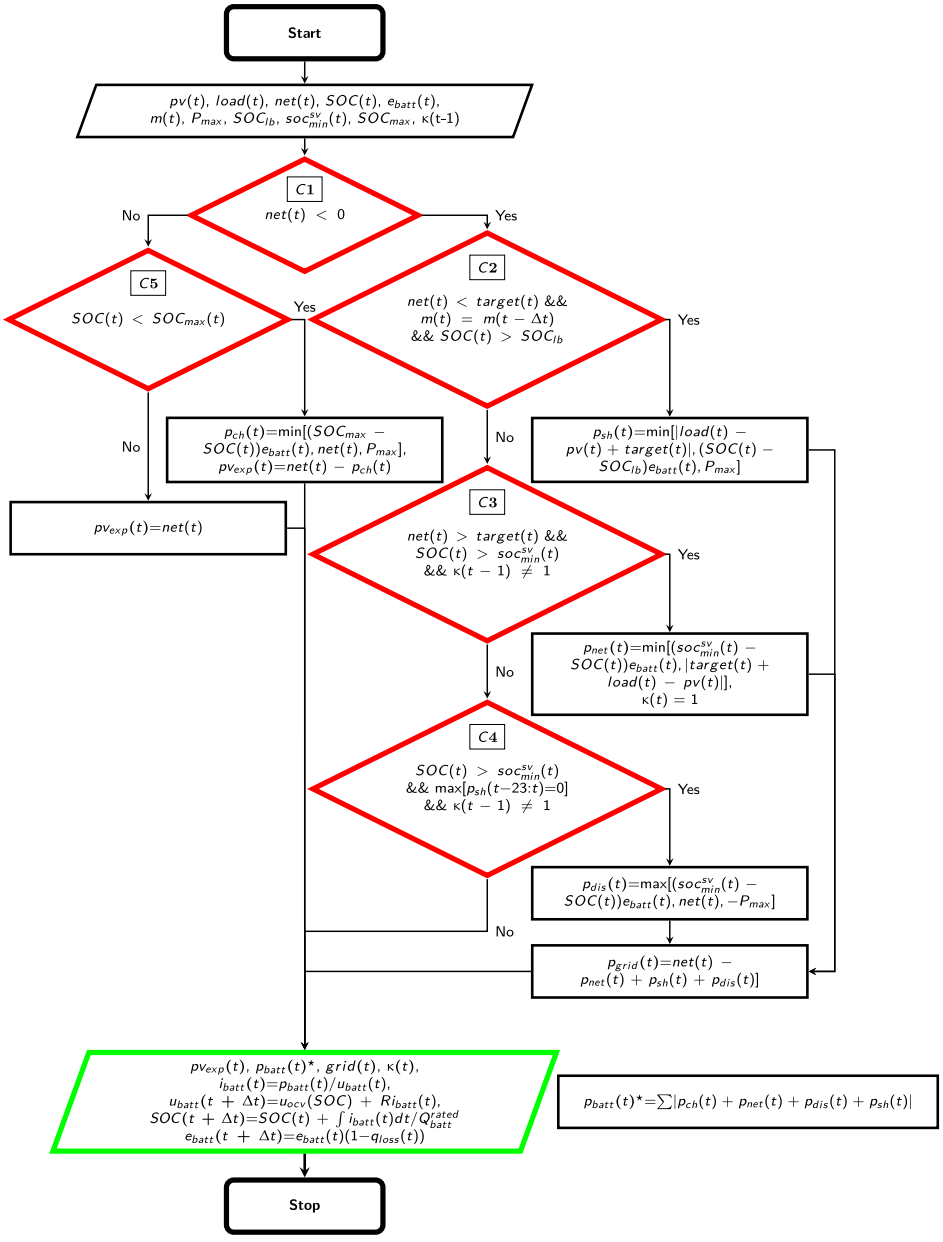

Fig. A.17. Flow chart of battery charge and discharge control for rule-based multi-objective (MO) dispatch.

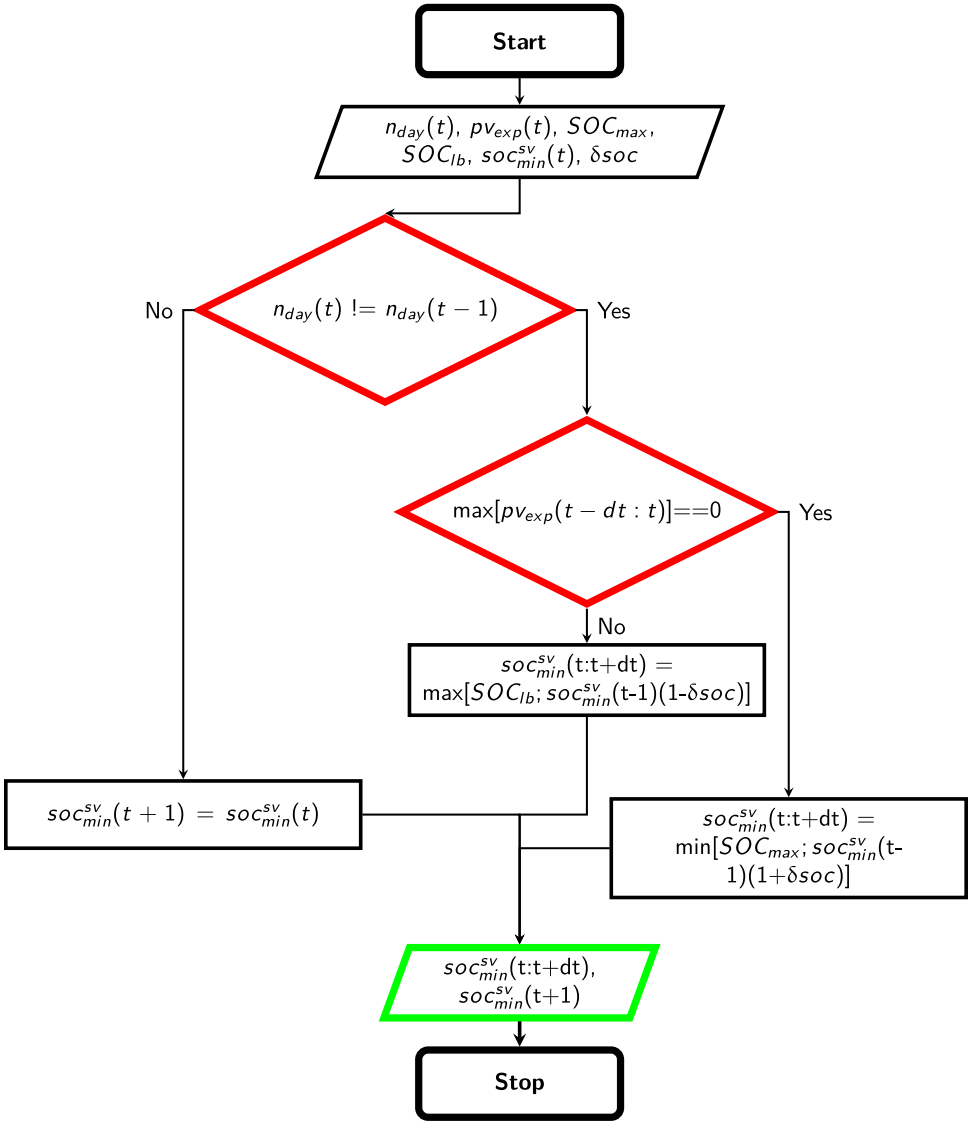

Fig. A.18. Rule-based operation of the minimum state-of-charge variation, $soc^{sv}_{min}(t)$, used in Fig. A.17.

References

[1] European Commission. Reducing emissions from aviation. 2023, https://climate.ec.europa.eu/eu-action/transport-emissions/reducing-emissions-aviation_en#links. [Accessed 06 March 2023].

[2] International Civil Aviation Organization. Trends in emissions that affect climate change. 2023, https://www.icao.int/environmental-protection/Pages/ClimateChange_Trends.aspx. [Accessed 06 March 2023].

[3] Cristea AD. The role of aviation networks for urban development. J Reg Sci 2017. http://dx.doi.org/10.1111/jors.12645.

[4] Graver B, Rutherford D, Zheng S. Co2 emissions from commercial aviation 2013, 2018, and 2019. Tech. rep., The International Council on Clean Transportation; 2020.

[5] Budd T, Budd L, Ison S. Environmentally sustainable practices at UK airports. In: Proceedings of the institution of civil engineers-transport, vol. 168. Thomas Telford Ltd; 2015, p. 116–23. http://dx.doi.org/10.1680/tran.13.00076.

[6] Kaya SK, Erginel N. Futuristic airport: A sustainable airport design by integrating hesitant fuzzy SWARA and hesitant fuzzy sustainable quality function deployment. J Clean Prod 2020;275:123880. http://dx.doi.org/10.1016/j.jclepro.2020.123880.

[7] Santa SLB, Ribeiro JMP, Mazon G, Schneider J, Barcelos RL, de Andrade JBSO, et al. A Green Airport model: Proposition based on social and environmental management systems. Sustainable Cities Soc 2020;59:102160. http://dx.doi.org/10.1016/j.scs.2020.102160.

[8] Schäfer AW, Barrett SR, Doyme K, Dray LM, Gnadt AR, Self R, et al. Technological, economic and environmental prospects of all-electric aircraft. Nat Energy 2019;4(2):160–6. http://dx.doi.org/10.1038/s41560-018-0294-x.

[9] Hou B, Bose S, Haran K. Powering electric aircraft at o'hare airport: A case study. In: 2020 IEEE power & energy society general meeting. IEEE; 2020, p. 1–5. http://dx.doi.org/10.1109/PESGM41954.2020.9281871.

[10] Jiang M, Qi L, Yu Z, Wu D, Si P, Li P, et al. National level assessment of using existing airport infrastructures for photovoltaic deployment. Appl Energy 2021;298:117195. http://dx.doi.org/10.1016/j.apenergy.2021.117195.

[11] Sukumaran S, Sudhakar K. Fully solar powered airport: A case study of cochin international airport. J Air Transp Manag 2017;62:176–88. http://dx.doi.org/10.1016/j.jairtraman.2017.04.004.

[12] Baek S, Kim H, Chang HJ. Optimal hybrid renewable airport power system: Empirical study on Incheon International Airport, South Korea. Sustainability 2016;8(6):562. http://dx.doi.org/10.3390/su8060562.

[13] Baxter G, Srisaeng P, Wild G. Environmentally sustainable airport energy management using solar power technology: The case of Adelaide Airport, Australia. Int J Traffic Transp Eng 2019;9(1). http://dx.doi.org/10.7708/ijtte.2019.9(1).07.

[14] Xiang Y, Cai H, Liu J, Zhang X. Techno-economic design of energy systems for airport electrification: A hydrogen-solar-storage integrated microgrid solution. Appl Energy 2021;283:116374. http://dx.doi.org/10.1016/j.apenergy.2020.116374.

[15] Brelje BJ, Martins JR. Electric, hybrid, and turboelectric fixed-wing aircraft: A review of concepts, models, and design approaches. Prog Aerosp Sci 2019;104:1–19. http://dx.doi.org/10.1016/j.paerosci.2018.06.004.

[16] Micallef A, Guerrero JM, Vasquez JC. New horizons for microgrids: From rural electrification to space applications. Energies 2023;16(4):1966. http://dx.doi.org/10.3390/en16041966.

[17] Guo Z, Li B, Taylor G, Zhang X. Infrastructure planning for airport microgrid integrated with electric aircraft and parking lot electric vehicles. eTransportation 2023;100257. http://dx.doi.org/10.1016/j.etran.2023.100257.

[18] Jin S, Li Y. Analyzing the performance of electricity, heating, and cooling supply nexus in a hybrid energy system of airport under uncertainty. Energy 2023;272:127138. http://dx.doi.org/10.1016/j.energy.2023.127138.

[19] Alruwaili M, Cipcigan L. Optimal annual operational cost of a hybrid renewable-based microgrid to increase the power resilience of a critical facility. Energies 2022;15(21):8040. http://dx.doi.org/10.3390/en15218040.

[20] Zhao H, Xiang Y, Shen Y, Guo Y, Xue P, Sun W, et al. Resilience assessment of hydrogen-integrated energy system for airport electrification. IEEE Trans Ind Appl 2021;58(2):2812–24. http://dx.doi.org/10.1109/TIA.2021.3127481.

[21] Trainelli L, Salucci F, Riboldi CE, Rolando A, Bigoni F. Optimal sizing and operation of airport infrastructures in support of electric-powered aviation. Aerospace 2021;8(2):40. http://dx.doi.org/10.3390/aerospace8020040.

[22] Ollas P, Persson J, Kovacs P. Effect of energy storage on self-consumption and self-sufficiency: A field study in a nordic climate. In: 38th European photovoltaic solar energy conference and exhibition. 2021, p. 1459–63. http://dx.doi.org/10.4229/EUPVSEC20212021-6BV.5.16.

[23] Zhang Y, Lundblad A, Campana PE, Benavente F, Yan J. Battery sizing and rule-based operation of grid-connected photovoltaic-battery system: A case study in Sweden. Energy Convers Manage 2017;133:249–63. http://dx.doi.org/10.1016/j.enconman.2016.11.060.

[24] Stephan A, Battke B, Beuse MD, Clausdeinken JH, Schmidt TS. Limiting the public cost of stationary battery deployment by combining applications. Nat Energy 2016;1(7):1–9. http://dx.doi.org/10.1038/nenergy.2016.79.

[25] Han X, Garrison J, Hug G. Techno-economic analysis of PV-battery systems in Switzerland. Renew Sustain Energy Rev 2022;158:112028. http://dx.doi.org/10.1016/j.rser.2021.112028.

[26] Seward W, Qadrdan M, Jenkins N. Revenue stacking for behind the meter battery storage in energy and ancillary services markets. Electr Power Syst Res 2022;211:108292. http://dx.doi.org/10.1016/j.epsr.2022.108292.

[27] Englberger S, Jossen A, Hesse H. Unlocking the potential of battery storage with the dynamic stacking of multiple applications. Cell Rep Phys Sci 2020;1(11):100238. http://dx.doi.org/10.1016/j.xcrp.2020.100238.

[28] Johnson V. Battery performance models in ADVISOR. J Power Sources 2002;110(2):321–9. http://dx.doi.org/10.1016/S0378-7753(02)00194-5.

[29] Plett GL. Extended Kalman filtering for battery management systems of LiPB-based HEV battery packs: Part 3. State and parameter estimation. J Power Sources 2004;134(2):277–92. http://dx.doi.org/10.1016/j.jpowsour.2004.02.033.

[30] Ollas P, Thiringer T, Persson M, Markusson C. Battery loss prediction using various loss models: A case study for a residential building. J Energy Storage 2023;70:108048. http://dx.doi.org/10.1016/j.est.2023.108048.

[31] Mohammadi F. Lithium-ion battery state-of-charge estimation based on an improved Coulomb-counting algorithm and uncertainty evaluation. J Energy Storage 2022;48:104061. http://dx.doi.org/10.1016/j.est.2022.104061.

[32] Collath N, Tepe B, Englberger S, Jossen A, Hesse H. Aging aware operation of lithium-ion battery energy storage systems: A review. J Energy Storage 2022;55:105634. http://dx.doi.org/10.1016/j.est.2022.105634.

[33] Bloom I, Cole B, Sohn J, Jones SA, Polzin EG, Battaglia VS, et al. An accelerated calendar and cycle life study of Li-ion cells. J Power Sources 2001;101(2):238–47. http://dx.doi.org/10.1016/S0378-7753(01)00783-2.

[34] Wang J, Liu P, Hicks-Garner J, Sherman E, Soukiazian S, Verbrugge M, et al. Cycle-life model for graphite-LiFePO4 cells. J Power Sources 2011;196(8):3942–8. http://dx.doi.org/10.1016/j.jpowsour.2010.11.134.

[35] Guo N, Zhang X, Zou Y, Guo L, Du G. Real-time predictive energy management of plug-in hybrid electric vehicles for coordination of fuel economy and battery degradation. Energy 2021;214:119070. http://dx.doi.org/10.1016/j.energy.2020.119070.

[36] Hu X, Zou C, Tang X, Liu T, Hu L. Cost-optimal energy management of hybrid electric vehicles using fuel cell/battery health-aware predictive control. IEEE Trans Power Electron 2019;35(1):382–92. http://dx.doi.org/10.1109/TPEL.2019.2915675.

[37] Zhang L, Hu X, Wang Z, Sun F, Deng J, Dorrell DG. Multiobjective optimal sizing of hybrid energy storage system for electric vehicles. IEEE Trans Veh Technol 2017;67(2):1027–35. http://dx.doi.org/10.1109/TVT.2017.2762368.

[38] Xie S, Hu X, Zhang Q, Lin X, Mu B, Ji H. Aging-aware co-optimization of battery size, depth of discharge, and energy management for plug-in hybrid electric vehicles. J Power Sources 2020;450:227638. http://dx.doi.org/10.1016/j.jpowsour.2019.227638.

[39] Luthander R, Widén J, Nilsson D, Palm J. Photovoltaic self-consumption in buildings: A review. Appl Energy 2015;142:80–94. http://dx.doi.org/10.1016/j.apenergy.2014.12.028.

[40] Ollas P, Persson J, Markusson C, Alfadel U. Impact of battery sizing on self-consumption, self-sufficiency and peak power demand for a low energy single-family house with PV production in Sweden. In: 2018 IEEE 7th world conference on photovoltaic energy conversion (WCPEC) (a joint conference of 45th IEEE PVSC, 28th PVSEC & 34th EU PVSEC). IEEE; 2018, p. 0618–23. http://dx.doi.org/10.1109/PVSC.2018.8548275.

[41] Alfredsson H, Nyman J, Nilsson J, Staack I. Infrastructure modeling for large-scale introduction of electric aviation. In: 35th International electric vehicle symposium and exhibition. 2022.

[42] European Aviation Safety Agency. Certification specifications for normal, utility, aerobatic, and commuter category aeroplanes CS–23. 2009.

[43] Swedavia Airports. Flygstatistik. 2023, https://www.swedavia.se/om-swedavia/statistik/. [Online accessed 03 March 2023].

[44] Qian K, Fachrizal R, Munkhammar J, Ebel T, Adam R. The impact of considering state of charge dependent maximum charging powers on the optimal electric vehicle charging scheduling. IEEE Trans Transp Electr 2023. http://dx.doi.org/10.1109/TTE.2023.3245332.

[45] Sreenath S, Sudhakar K, Yusop A, Cuce E, Solomin E. Analysis of solar PV glare in airport environment: Potential solutions. Results Eng 2020;5:100079. http://dx.doi.org/10.1016/j.rineng.2019.100079.

[46] Sreenath S, Sudhakar K, Yusop AF. Airport-based photovoltaic applications. Prog Photovolt, Res Appl 2020;28(8):833–53. http://dx.doi.org/10.1002/pip.3265.

[47] Sreenath S, Sudhakar K, Yusop A. Solar photovoltaics in airport: Risk assessment and mitigation strategies. Environ Impact Assess Rev 2020;84:106418. http://dx.doi.org/10.1016/j.eiar.2020.106418.

[48] Barrett S, DeVita P. Technical guidance for evaluating selected solar technologies on airports. Washington, ABD: Federal Aviation Administration; 2018.

[49] aurora. HelioScope. 2022, URL https://helioscope.aurorasolar.com.

[50] Ollas P, Thiringer T, Persson M, Markusson C. Energy loss savings using direct current distribution in a residential building with solar photovoltaic and battery storage. Energies 2023;16(3):1131. http://dx.doi.org/10.3390/en16031131.

[51] Fares RL, Webber ME. The impacts of storing solar energy in the home to reduce reliance on the utility. Nat Energy 2017;2(2):1–10. http://dx.doi.org/10.1038/nenergy.2017.1.

[52] Hanna R, Kleissl J, Nottrott A, Ferry M. Energy dispatch schedule optimization for demand charge reduction using a photovoltaic-battery storage system with solar forecasting. Sol Energy 2014;103:269–87. http://dx.doi.org/10.1016/j.solener.2014.02.020.

[53] Moshövel J, Kairies K-P, Magnor D, Leuthold M, Bost M, Gährs S, et al. Analysis of the maximal possible grid relief from PV-peak-power impacts by using storage systems for increased self-consumption. Appl Energy 2015;137:567–75. http://dx.doi.org/10.1016/j.apenergy.2014.07.021.

[54] Campana PE, Cioccolanti L, François B, Jurasz J, Zhang Y, Varini M, et al. Li-ion batteries for peak shaving, price arbitrage, and photovoltaic self-consumption in commercial buildings: A Monte Carlo analysis. Energy Convers Manage 2021;234:113889. http://dx.doi.org/10.1016/j.enconman.2021.113889.

[55] Nyholm E, Goop J, Odenberger M, Johnsson F. Solar photovoltaic-battery systems in Swedish households–self-consumption and self-sufficiency. Appl Energy 2016;183:148–59. http://dx.doi.org/10.1016/j.apenergy.2016.08.172.

[56] Widén J, Wäckelgård E, Lund PD. Options for improving the load matching capability of distributed photovoltaics: Methodology and application to high-latitude data. Sol Energy 2009;83(11):1953–66. http://dx.doi.org/10.1016/j.solener.2009.07.007.

[57] Ollas P. Energy savings using a direct-current distribution network in a PV and battery equipped residential building [Lic. thesis], Sweden: Chalmers University of Technology; 2020.

[58] NordPool. Day-ahead prices. 2023, https://www.nordpoolgroup.com/en/Market-data1/Dayahead/Area-Prices/ALL1/Hourly/?view=table. [Online accessed 03 March 2023].

[59] Lindahl J, Oller Westerberg A, K. V. National survey report of PV power applications in Sweden 2020. International Energy Agency (IEA); 2021.

[60] Feldman D, Ramasamy V, Fu R, Ramdas A, Desai J, Margolis R. US solar photovoltaic system and energy storage cost benchmark (Q1 2020). Tech. rep., Golden, CO (United States): National Renewable Energy Lab.(NREL); 2021.

[61] García-Miguel PLC, Alonso-Martínez J, Arnaltes Gómez S, García Plaza M, Asensio AP. A review on the degradation implementation for the operation of battery energy storage systems. Batteries 2022;8(9):110. http://dx.doi.org/10.3390/batteries8090110.

[62] Calearo L, Marinelli M. Profitability of frequency regulation by electric vehicles in Denmark and Japan considering battery degradation costs. World Electr Veh J 2020;11(3):48. http://dx.doi.org/10.3390/wevj11030048.

[63] Lai CS, Jia Y, Xu Z, Lai LL, Li X, Cao J, et al. Levelized cost of electricity for photovoltaic/biogas power plant hybrid system with electrical energy storage degradation costs. Energy Convers Manage 2017;153:34–47. http://dx.doi.org/10.1016/j.enconman.2017.09.076.

[64] Ahmadian A, Sedghi M, Mohammadi-ivatloo B, Elkamel A, Golkar MA, Fowler M. Cost-benefit analysis of V2G implementation in distribution networks considering PEVs battery degradation. IEEE Trans Sustain Energy 2017;9(2):961–70. http://dx.doi.org/10.1109/TSTE.2017.2768437.

[65] Hou Q, Yu Y, Du E, He H, Zhang N, Kang C, et al. Embedding scrapping criterion and degradation model in optimal operation of peak-shaving lithium-ion battery energy storage. Appl Energy 2020;278:115601. http://dx.doi.org/10.1016/j.apenergy.2020.115601.

[66] Cai J, Zhang H, Jin X. Aging-aware predictive control of PV-battery assets in buildings. Appl Energy 2019;236:478–88. http://dx.doi.org/10.1016/j.apenergy.2018.12.003.

[67] Cao J, Harrold D, Fan Z, Morstyn T, Healey D, Li K. Deep reinforcement learning-based energy storage arbitrage with accurate lithium-ion battery degradation model. IEEE Trans Smart Grid 2020;11(5):4513–21. http://dx.doi.org/10.1109/TSG.2020.2986333.

[68] Awad H, Gül M. Load-match-driven design of solar PV systems at high latitudes in the northern hemisphere and its impact on the grid. Sol Energy 2018;173:377–97. http://dx.doi.org/10.1016/j.solener.2018.07.010.
[69] Wikner E, Thiringer T. Extending battery lifetime by avoiding high SOC. Appl Sci 2018;8(10):1825. http://dx.doi.org/10.3390/app8101825.
[70] Zia MF, Elbouchikhi E, Benbouzid M. Optimal operational planning of scalable DC microgrid with demand response, islanding, and battery degradation cost considerations. Appl Energy 2019;237:695–707. http://dx.doi.org/10.1016/j.apenergy.2019.01.040.